

# Colossal Dielectric Response and Electric Polarization in Lithium Nitrate

Na Du,<sup>†</sup> Yan Zhao,<sup>†</sup> Enting Xu,<sup>†</sup> Jianwei Han, Peng Ren,<sup>\*</sup> Fei Yen<sup>\*</sup>

*School of Science, Harbin Institute of Technology, Shenzhen,  
University Town, Shenzhen, Guangdong 518055, P. R. China.*

## **Corresponding Author:**

\*E-mail: fyen@hit.edu.cn, renpeng@hit.edu.cn

<sup>†</sup>These authors contributed equally to this work

**Abstract:** Materials with record-breaking properties are interesting as they can redefine existing models. Lithium nitrate  $\text{LiNO}_3$  is identified to possess a dielectric constant  $\epsilon'$  larger than  $6 \times 10^6$  at 1 kHz in powdered samples above the critical temperature  $T_W = 306$  K. When cooling back from  $T_W$ , if the temperature remains above 275 K,  $\epsilon'$  can be sustained above  $10^4$  and the dissipation factor below  $10^2$ . Moreover, pyroelectric current measurements show  $\text{LiNO}_3$  to be ferroelectric with an electric polarization of  $P = \pm 1,200 \mu\text{C}/\text{cm}^2$ . Both  $\epsilon'$  and  $P$  are the highest amongst all known materials. We suggest the mechanism underlying the colossal magnitudes of  $\epsilon'$  and  $P$  to stem from a gearing-ungearing process of the planar  $\text{NO}_3^-$  at the macroscopic level. Our results potentially push the boundaries of ceramic capacitors.

**Keywords:** giant permittivity, ferroelectricity, dielectrics, order-disorder phenomena, phase transitions

Lithium nitrate  $\text{LiNO}_3$  crystallizes in the trigonal structure [1-3]. According to Strømme [1], the packing of the rhombohedral lattice along with all of the O–O distances requires that the planar  $\text{NO}_3^-$  ions are spatially ordered. As such, it was suggested that  $\text{LiNO}_3$  is the only univalent nitrate  $\text{XNO}_3$  (where  $X = \text{Li, Na, NH}_4, \text{K, Rb, Cs, Ag and Tl}$ ) that does not possess a spatially disordered solid phase so an order-disorder phase transition is not expected to occur. However, we recently observed a reversible solid-solid phase transition in  $\text{LiNO}_3$  according to experimental measurements of the magnetic susceptibility [4]. It was believed that the librations (the in-plane, back-and-forth rocking) of neighboring  $\text{NO}_3^-$  become geared below  $T_C = 265$  K and ungeared above  $T_W = 303$  K. Note the associated hysteresis spans nearly 40 K. Fermor & Kjekshus also reported on a phase transition at 263 K during cooling but their warming data stopped at 296 K, just short of  $T_W$  [5]. The dielectric constant data of Fermor & Kjekshus were rather sparse, varying from 3 K to 10 K per data point and the sweeping speed was also not reported. It was therefore of general interest to re-investigate the dielectric properties of  $\text{LiNO}_3$  in the range of 200–330 K under slow and constant sweeping rates.

To our surprise, the measured dielectric constant with respect to temperature  $\epsilon'(T)$  was observed to increase by around four orders of magnitude at  $T_W$  when samples were directly warmed from room temperature. This result renders  $\text{LiNO}_3$  as having one of the highest (if not the highest) dielectric constants ever reported. Materials with a giant dielectric constant (GDC) have potential to be employed as dielectrics for energy storage and actuators having nonlinear opto-electronic effects. Many types of materials with GDC exist such as ceramics [6], high entropy alloys [7], plastic crystals [8] and photo-induced organic-inorganic perovskites [9]. The mechanisms underlying GDC are also diverse: they include ferroelectricity [10,11], polaron hopping [12], grain boundary [13] and electrode interfacial effects [14]. In the case of  $\text{LiNO}_3$ , we suggest the observed GDC to stem from an isostructural first-order phase transition involving the gearing-ungearing process of the  $\text{NO}_3^-$  ions.

In this work, we present data on  $\epsilon'(T)$  along with the imaginary part of the dielectric constant  $\epsilon''(T)$  under 1 kHz in the range of 200 to 380 K. The complex dielectric constant at 310 K in the frequency range of 20 Hz to 300 kHz is also presented. Large dielectric constants often correlate to ferroelectricity [15] so measurements of the pyroelectric current were also carried out. We find a record high electric polarization that can be switched according to the polarity of a *dc* external electric field characterizing LiNO<sub>3</sub> as ferroelectric. Lastly, we discuss a possible mechanism leading to the observed colossal dielectric response and electric polarization.

Lithium nitrate (CAS# 7790-69-4) 99.99% in purity was purchased from Aladdin, Inc., Macklin, Inc. and Meryer, Inc. For the samples labelled 'powdered', the reagent was used 'as is' (with no further purification), taken directly from the bottle and pressed into disc pellets having diameters of 3.00 mm and thicknesses of 0.38 to 0.44 mm. Silver paint electrodes were applied onto the two flat surfaces of the pellets to form a parallel plate capacitor having platinum wire leads. The real and imaginary parts of the dielectric constant were obtained from the measured capacitance and dissipation factor, respectively, with an Agilent A4980E impedance analyzer. Temperature control and thermometry were realized with the cryostat of a PPMS system manufactured by Quantum Design, Inc.

For the single crystalline samples, a solution of LiNO<sub>3</sub>+H<sub>2</sub>O was slowly evaporated. Large, flat, transparent and trigonal-shaped crystals were then harvested. The pyroelectric current was measured by a Keithley 4917B electrometer. The crystal structure was drawn using the freeware Visualization for Electronic and Structural Analysis (VESTA) v3.4.6 [16].

Figures 1a and 1b show  $\epsilon'(T)$  and  $\epsilon''(T)$ , respectively, of LiNO<sub>3</sub> under 1 kHz during warming from 300 K to 310 K from three providers. Near 306 K  $\epsilon'(T)$  increased dramatically by nearly four orders of magnitude in the span of 5 K to reach values near  $7 \times 10^6$ . The behavior of  $\epsilon''(T)$  followed the same pattern and possessed nearly the same

order of magnitude at temperatures above 307 K. Figure 1c shows the same  $\epsilon'(T)$  scans but under different frequencies.  $\epsilon''(T)$  exhibited a similar profile so instead the dissipation factor ( $\tan \delta = \epsilon'' / \epsilon'$ ) is shown in Fig. 1d. The largest observed  $\epsilon'$  was  $\sim 2 \times 10^8$  at 306.7 K under 25 Hz. The values in parenthesis in Fig. 1a show the thicknesses of the disc-shaped samples (inset of Fig. 1b). Given that  $\epsilon'$  was relatively independent of sample thickness indicates the colossal response of  $\epsilon'$  is mostly a bulk effect.

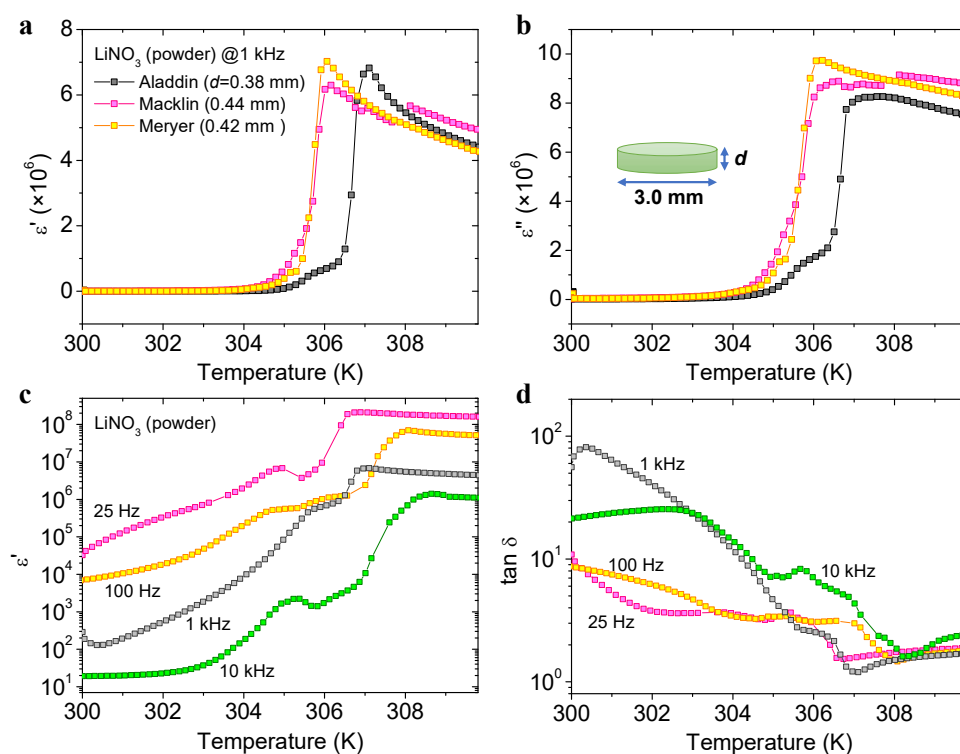


**Fig. 1.** (a) Real  $\epsilon'(T)$  and (b) Imaginary  $\epsilon''(T)$  parts of the dielectric constant of  $\text{LiNO}_3$  (powder pressed into pellet) under 1 kHz during warming (1 K/min) from three manufacturers. Inset shows the dimensions and shape of the pellets. (c)  $\epsilon'(T)$  under different frequencies. (d) Dissipation factor  $\tan \delta = \epsilon'' / \epsilon'$  against temperature.

Figures 2a and 2b show  $\epsilon'(T)$  and  $\epsilon''(T)$  of one sample subjected to successive warming and cooling cycles under 1 kHz in a larger temperature range. In general, both  $\epsilon'(T)$  and  $\epsilon''(T)$  followed a similar behavior. Here, the most pronounced feature is again the sharp increase by orders of magnitude near  $T_w$  during the warming runs. The sudden increase of  $\epsilon'(T)$  and  $\epsilon''(T)$  of the latter two warming runs were less pronounced but they occurred at nearly the same temperature. From the cooling curves in Figs. 2a and 2b, the disorder-order transition temperature can also be discerned to occur near  $T_c = 275$

K where  $\epsilon'(T)$  and  $\epsilon''(T)$  exhibited a sudden drop by many orders of magnitude. After many repetitions with different samples, we find that  $T_W$  varies only between 304.7 and 307.0 K while  $T_C$  can vary between 262.0 to 275.5 K. For practical applications, once the temperature is warmed above  $T_W$  to 'activate' the colossal magnitude of  $\epsilon'$ , its value can be kept to remain above  $10^4$  if the temperature is maintained above 275 K.

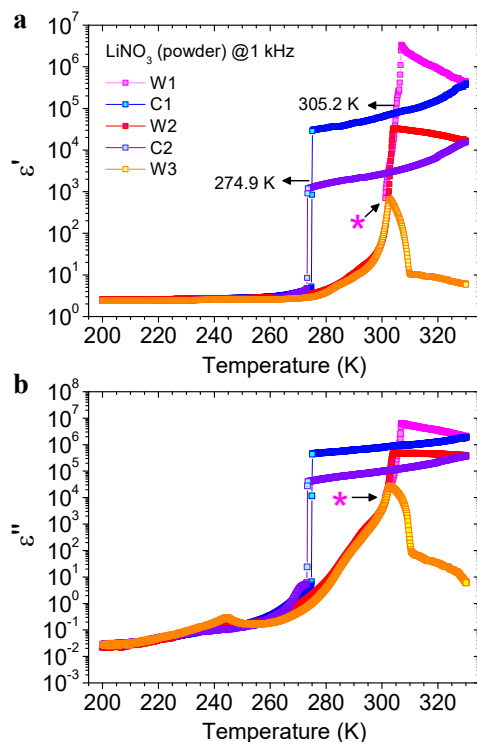


**Fig. 2.** (a)  $\epsilon'(T)$  and (b)  $\epsilon''(T)$  of  $\text{LiNO}_3$  (powder) under 1 kHz subjected to three warming and two cooling cycles all at 1 K/min. The \* symbol indicates the start of the experiments.

Sharp changes in  $\epsilon'(T)$  and  $\epsilon''(T)$  usually pertain to structural phase transitions. To rule out whether this is the case in  $\text{LiNO}_3$ , XRD measurements were performed on single crystalline samples at 100 K, 240 K and 380 K (results are shown in the Supplementary Material). At all three temperatures the crystal structure of  $\text{LiNO}_3$  was confirmed to be trigonal (Space group No. 167) in agreement with existing literature [1-3]. From such, the large magnitudes of  $\epsilon'(T)$  and  $\epsilon''(T)$  appear to mainly represent the structural dynamics of the system; more specifically, the frequencies of the  $\text{NO}_3^-$  librations at different temperatures. This will be discussed in more detail below. The packing of the unit lattice is also consistent with Strømme's (1970) conclusion that no

*spatial* order-disorder takes place in the solid state of  $\text{LiNO}_3$  [1]. Therefore, the most plausible scenario we can think of is to presume the observed phase transition to be associated to a *temporal* order-disorder (gearing-ungearing) of the  $\text{NO}_3^-$  according to our previous results [4,17], *i.e.* the anions librate independently from each other in the disordered phase, and in contrast to the ordered phase, the intermolecular librations become coherent. In the Supplementary Material file, results of the measured specific heat across  $T_W$  is also included. A small  $\lambda$ -peak anomaly was identified which further verifies the order-disorder nature of the phase transition.

Figures 3a to 3d show the complex dielectric constant as functions of frequency  $f$  of  $\text{LiNO}_3$  at 310 K just after crossing  $T_W$ . Both  $\epsilon'(\omega)$  and  $\epsilon''(\omega)$  (where  $\omega = 2\pi f$ ) behaved monotonically between 20 Hz and 300 kHz, the limits of our impedance analyzer. The largest observed value of  $\epsilon'$  was  $>1 \times 10^8$  at 20 Hz. The insets in Figs. 3b and 3d show  $\tan \delta$  as a function of frequency. At frequencies below 1 kHz,  $\tan \delta$  was in the low single digits. Such a colossal value of  $\epsilon'$  coupled to a relatively small  $\tan \delta$  makes  $\text{LiNO}_3$  an attractive candidate for insulation layers in nanoscale electronics.

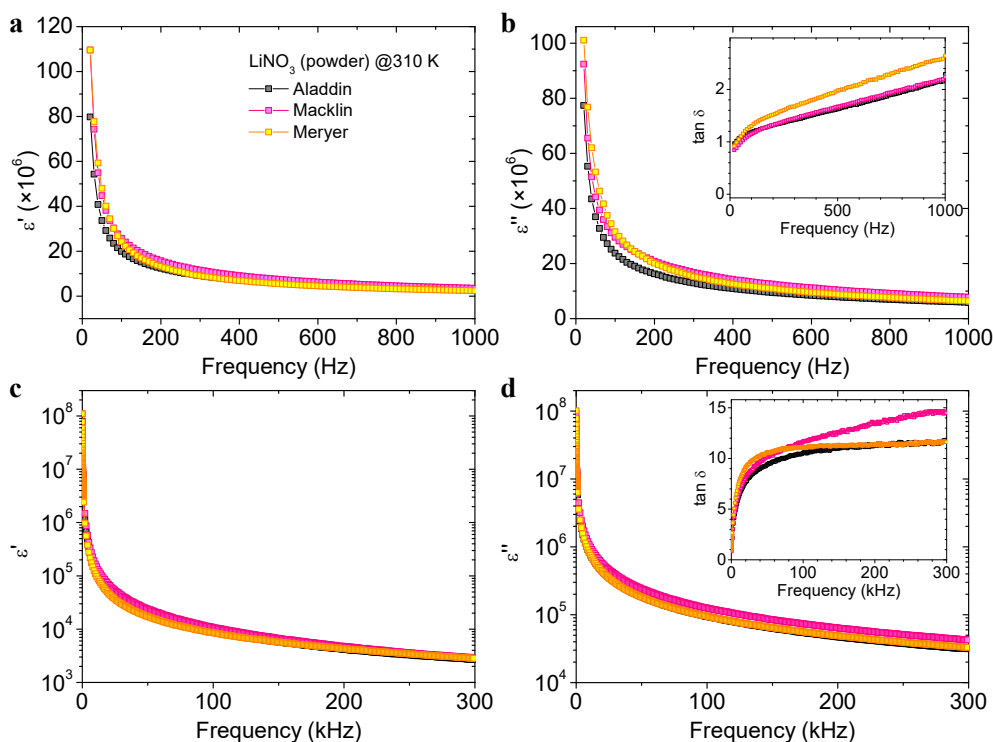


**Fig. 3.** Complex dielectric constant as a function of frequency of  $\text{LiNO}_3$  at 310 K in the (a), (b) near-static range and (c), (d) up to 300 kHz. Insets also show  $\tan \delta$  against

frequency.

Figure 4a shows the measured pyroelectric current of a single crystalline sample along the direction perpendicular to the  $c$ -axis. A  $dc$  electric field of  $E = +555.6$  V/cm was applied to the sample at 330 K which was then cooled down to 260 K. The electric field was removed and the sample was warmed back to 330 K at the rate of 2 K/min while recording any measured current. This pyroelectric current  $I(T)$  is shown in red in Fig. 4a. Immediately afterwards,  $E = -555.6$  V/cm was applied to the sample and the abovementioned process was repeated with the recorded  $I(T)$  shown in blue.

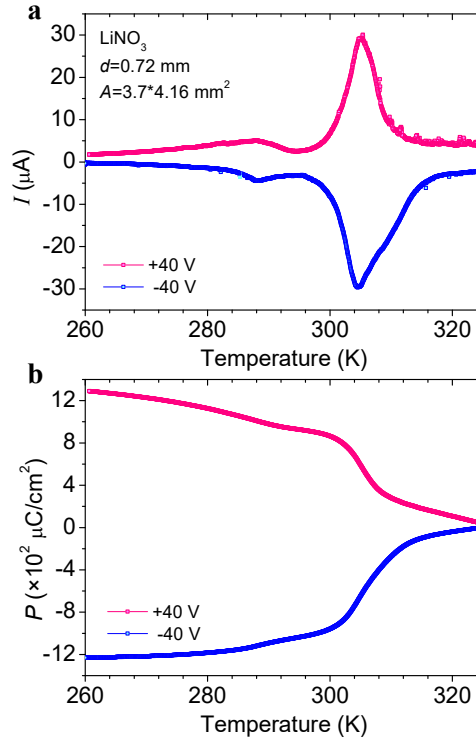


**Fig. 4.** (a) Measured pyroelectric current  $I(T)$  of  $\text{LiNO}_3$  with thickness  $d$  and area  $A$  at 2 K/min. A  $dc$  electric field of  $\pm 555.6$  V/cm was applied when the sample was cooled to 260 K before each measurement. (b) Derived electric polarization from integration of  $I(T)$ .

In both of the  $I(T)$  curves a peak was observed near 305.5 K which was in good agreement with the  $\epsilon'(T)$  and  $\epsilon''(T)$  data (Fig. 2). The area below each  $I(T)$  curve is proportional to the electric polarization of the sample (shown in Fig. 4b). An unprecedented value of  $\sim 1,200 \mu\text{C}/\text{cm}^2$  was recorded. As a comparison, the highest recorded polarizations have only been just above  $100 \mu\text{C}/\text{cm}^2$  [18-20].

The fact that the electric polarization can be switched according to an external applied electric field characterizes the low temperature ordered phase of  $\text{LiNO}_3$  as ferroelectric. It should be noted that  $P$ - $E$  measurements were also carried out at temperatures below  $T_C$  but a remnant polarization was not observed. This is consistent with ferroelectrics of type-II as  $P$ - $E$  hysteresis loops are usually only observable in type-I (displacive) ferroelectrics [21].

As mentioned above, the magnitude of  $\epsilon'(T)$  is proportional to the rate of libration of the  $\text{NO}_3^-$ . Hence, a natural question to ask is why do the  $\text{NO}_3^-$  exhibit the type of observed dynamics? We first note that all  $\text{NO}_3^-$  reside in an equilateral triangular lattice along the  $ab$ -planes (Fig. 5a). Moreover, the stacking of the  $ab$ -planes is in such a way that the positions of each  $\text{NO}_3^-$  is exactly above the center of three  $\text{NO}_3^-$  below. This means that each  $\text{NO}_3^-$  is equidistant by  $a_N$  to six  $\text{NO}_3^-$  within the same  $ab$ -plane and equidistant by  $c_N$  to six other  $\text{NO}_3^-$  at different  $z$  (three above and three below). Figure 5b also lists the values of  $a_N$  and  $c_N$  of  $\text{LiNO}_3$  at 380 K, 240 K and 100 K. At high temperatures ( $\sim 380$  K), the  $\text{NO}_3^-$  librate independently from each other, however, at low temperatures (at low enough thermal fluctuations) neighboring anions become correlated because of conservation of angular momentum. For instance, if there were only two anions in the ground state with minimal fluctuations, as one  $\text{NO}_3^-$  rotates by  $\theta$ , then the other must do so by  $-\theta$  (similar to Huygen's clocks) [22,23]. A problem appears as  $\text{LiNO}_3$  is cooled because of its near-perfect triangular lattice. Once two adjacent  $\text{NO}_3^-$  have become geared, a third equidistant  $\text{NO}_3^-$  does not know whether to become correlated to the first or second  $\text{NO}_3^-$  (Fig. 5b). Such geometric frustration is similar to that encountered in conventional magnetic systems where the spin of an unpaired electron equidistant to two others does not know whether to point up or down [24-26]. To remedy this situation, the lighter ion becomes off-centered because the high temperature phase is spatially disordered or because there are two types of anions such as in  $\text{NH}_4(\text{SO}_4)_2$  [27]. However, Jahn-Teller-like distortions (at the molecular level) seem to be inhibited in  $\text{LiNO}_3$  because



of its unique near-perfect crystal lattice even at high temperatures. As neighboring  $\text{NO}_3^-$  librate closer and closer to each other's natural frequency with decreasing temperature the system enters into a highly critical state since the  $\text{NO}_3^-$  librate at each other's resonant frequency [28]. One solution to the sustained geometric frustration of the librations is that the  $\text{NO}_3^-$  within entire  $ab$ -planes rotate in-phase while that of adjacent planes are offset by  $180^\circ$  (antiphase). This may be the reason behind the observed 40 K hysteresis between  $T_W$  and  $T_C$  as a lot of negotiating between neighboring  $\text{NO}_3^-$  must take place in order for the entire system to become geared at a macroscopically level. The large hysteretic region is likely due to the system attempting to resolve its three-dimensional geometric frustration up until  $T_C$  where the sharp drop-offs in  $\epsilon'(T)$  and  $\epsilon''(T)$  signal the resolving of the issue.

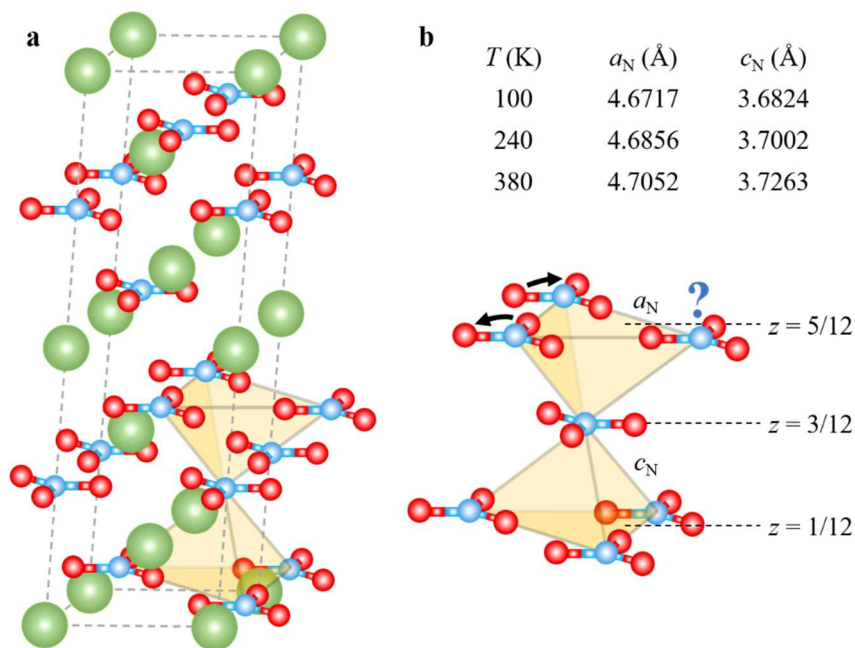


**Fig. 5.** (a) Crystal structure of  $\text{LiNO}_3$ . Parameters are available in the Supplementary Material. (b)  $\text{NO}_3^-$  ions illustrating the inherent geometric frustration along the  $ab$ -planes and  $c$ -axis in the studied temperatures of 100, 240 and 380 K.

As the system is warmed up, the  $\text{NO}_3^-$  librations remain geared up until  $T_W$  where the vibrations of the  $\text{Li}^+$  and/or  $\text{NO}_3^-$  ions (thermal fluctuations) apparently begin to disrupt the macroscopic coherent state of the anions. The phase transition at  $T_W$  is first order so the system first absorbs latent heat. This latent heat is usually used to change the structure of the system, however, the order-disorder phase transition in  $\text{LiNO}_3$  is

isostructural so the release of the absorbed latent heat seems to mostly be transferred onto the  $\text{NO}_3^-$  libration modes which causes the huge spikes observed in  $\epsilon'(T)$  and  $\epsilon''(T)$  at  $T_w$ .

Regarding the observed ferroelectricity, magnetic moments ordered into a spiral configuration can give rise to a spontaneous polarization [29,30]. This is possible because inversion of all magnetic moments along the propagation vector breaks the time-reversal and spatial-inversion symmetries. As each  $\text{NO}_3^-$  rotates from  $+\theta$  to  $-\theta$ , an equivalent magnetic moment perpendicular to the rotation plane is generated because the oxygen ions trace out current loops while the nitrogen atoms are near-stationary and the orbitals of the paired electrons cancel each other out. When the  $\text{NO}_3^-$  ion rotates back to  $+\theta$  from  $-\theta$ , the magnetic moment points along the opposite direction. If a phase shift  $\delta$  exists between adjacent gearing  $ab$ -planes, then the magnetic moments of the  $\text{NO}_3^-$  along the  $c$ -axis form spiral configurations. If the  $c$ -axis lattice constant is not a multiple of  $\delta$ , i.e.  $c / \delta$  is incommensurate, then the ordered phase of  $\text{LiNO}_3$  should exhibit a macroscopic polarization.

To conclude, while  $\text{LiNO}_3$  possesses a colossal electric polarization, its applications for memory storage are limited because the temperature must be varied widely. On the other hand, a colossal dielectric response and large operating temperature range (275 to 330 K) enables  $\text{LiNO}_3$  to potentially increase the performance of existing Class 2 ceramic capacitors, especially when the material is commercially available, inexpensive, light-weighted and environmentally friendly. The Supplementary Materials file also shows  $\epsilon'$  to be nearly independent of applied electric field from 0.6 to 25 V/cm. Lastly, a dissipation factor of  $10^0$ – $10^1$  at low frequencies also makes  $\text{LiNO}_3$  attractive for use in sub-micron electronics.

## References:

1. K. O. Strømme, On the crystal structure of lithium nitrate above room temperature, *Acta Chem. Scand.* **24**, 1479-1481 (1970).  
<https://doi.org/10.3891/acta.chem.scand.24-1479>
2. X. Wu, F. R. Fronczek, L. G. Burler, Structure of LiNO<sub>3</sub>: Point charge model and sign of the <sup>7</sup>Li quadrupole coupling constant, *Inorg. Chem.* **33**, 1363-1365 (1994).  
<https://doi.org/10.1021/ic00085a025>
3. J. Vinson, T. Jach, M. Müller, R. Unterumsberber, B. Beckhoff, Resonant x-ray emission and valence-band lifetime broadening in LiNO<sub>3</sub>, *Phys. Rev. B* **100**, 085143 (2019). <https://doi.org/10.1103/PhysRevB.100.085143>
4. N. Du, X. Wang, R. Wang, E. Xu, Y. Y. Zhu, Y. Zhao, P. Ren, F. Yen, Magnetism based on nitrate-nitrate interactions: The cases of LiNO<sub>3</sub>, K<sub>0.5</sub>Rb<sub>0.5</sub>NO<sub>3</sub>, Ca(NO<sub>3</sub>)<sub>2</sub> and C(NH<sub>2</sub>)<sub>3</sub>NO<sub>3</sub>, <https://arxiv.org/abs/2501.05754> (2025).
5. J. H. Fermor, A. Kjekshus, On the electrical properties of LiNO<sub>3</sub>, *Acta Chem. Scand.* **23**, 1581-1587 (1969). <https://doi.org/10.3891/acta.chem.scand.23-1581>
6. A. P. Ramirez, M. A. Subramanian, M. Gardel, G. Blumber, D. Li, T. Vogt, S. M. Shapiro, Giant dielectric constant response in a copper-titanate, *Solid State Comm.* **115**, 217-220 (2000). [https://doi.org/10.1016/S0038-1098\(00\)00182-4](https://doi.org/10.1016/S0038-1098(00)00182-4)
7. D. Bérardan, S. Franger, D. Dragoë, A. K. Meena, N. Dragoë, Colossal dielectric constant in high entropy oxides, *Phys. Status Solidi RRL* **10**, 328-333 (2016).  
<https://doi.org/10.1002/pssr.201600043>
8. P. Gonzalez-Izquierdo, O. Fabelo, L. Canadillas-Delgado, G. Beobide, O. Vallcorba, M. Sanchez-Andujar, M. T. Fernandez-Diaz, I. de Pedro, Temperature evolution of (quinuclidinium)[FeCl<sub>4</sub>]: a plastic/polar magnetic hybrid compound with giant dielectric constant, *J. Mat. Chem. C* **8**, 11389-11398 (2020).  
<https://doi.org/10.1039/D0TC02341H>
9. E. J. Juarez-Perez, R. S. Sanchez, L. Badia, G. Garcia-Belmonte, Y. S. Kang, I. Mora-Sero, J. Bisquert, Photoinduced giant dielectric constant in lead halide perovskite solar cells, *J. Phys. Chem. Lett.* **5**, 2390-2394 (2014).  
<http://doi.org/10.1021/jz5011169>
10. D. Fu, H. Cai, Y. Liu, Q. Ye, W. Zhang, Y. Zhang, X. Chen, G. Giovannetti, M. Capone, J. Li, R. Xiong, Diisopropylammonium bromide is a high-temperature molecular ferroelectric crystal, *Science* **339**, 425-428 (2013).  
<https://doi.org/10.1126/science.1229675>
11. T. Hirose, K. Furukawa, Dielectric anomaly of tungsten trioxide WO<sub>3</sub> with giant dielectric constant, *Phys. Status Solidi A* **203**, 608-615 (2006).  
<https://doi.org/10.1002/pssa.200521407>
12. V. Ligatchev, Polaronic phase transitions and complex permittivity of solid polar insulators with gigantic dielectric response, *Phys. Status Solidi B* **251**, 569-592 (2013). <https://doi.org/10.1002/pssb.201349262>
13. J. Wu, C. -W. Nan, Y. Lin, Y. Deng, Giant dielectric permittivity observed in Li and Ti doped NiO, *Phys. Rev. Lett.* **89**, 217601 (2002).  
<https://doi.org/10.1103/PhysRevLett.89.217601>

14. P. Lunkenheimer, R. Fichtl, S. G. Ebbinghaus, A. Loidl, Nonintrinsic origin of the colossal dielectric constants in  $\text{CaCu}_3\text{Ti}_4\text{O}_{12}$ , *Phys. Rev. B* **70**, 172102 (2004).  
<https://doi.org/10.1103/PhysRevB.70.172102>
15. F. Jona, G. Shirane, *Ferroelectric Crystals*, Pergamon Press Ltd.: Oxford, UK (1962).
16. K. Momma, F. Izumi, VESTA 3 for three-dimensional visualization of crystal, volumetric and morphology data, *J. Appl. Crystallogr.* **44**, 1272-1276 (2011).  
<https://doi.org/10.1107/S0021889811038970>
17. N. Du, X. Wang, Y. Y. Zhu, P. Ren, F. Yen, Gearing of nitrate ions in ammonium nitrate, *J. Chem. Phys.* accepted, (2025) <http://arxiv.org/abs/2501.02954>
18. D. Lebeugle, D. Colson, A. Forget, M. Viret, Very large spontaneous electric polarization in  $\text{BiFeO}_3$  single crystals at room temperature and its evolution under cycling fields, *Appl. Phys. Lett.* **91**, 022907 (2007).  
<https://doi.org/10.1063/1.2753390>
19. K. Y. Yun, D. Ricinschi, T. Kanashima, M. Noda, M. Okuyama, Giant ferroelectric polarization beyond  $150 \mu\text{C}/\text{cm}^2$  in  $\text{BiFeO}_3$  thin film, *Jpn. J. Appl. Phys.* **43**, L647 (2004). <https://doi.org/10.1143/JJAP.43.L647>
20. U. Chon, H. M. Jang, M. G. Kim, C. H. Chang, Layered perovskites with giant spontaneous polarizations for nonvolatile memories, *Phys. Rev. Lett.* **89**, 087601 (2002). <https://doi.org/10.1103/PhysRevLett.89.087601>
21. P. Peksa, A. Sieradzki, Controversy on the ferroelectricity in metal-formate frameworks, *Lithuanian J. Phys.* **62**, 195–205 (2022).  
<https://doi.org/10.3952/physics.v62i4.4814>
22. J. Peña Ramirez, K. Aihara, R. H. B. Fey, H. Nijmeijer, Further understanding of Huygens' coupled clocks: The effect of stiffness, *Physica D* **270**, 11-19 (2014).  
<https://doi.org/10.1016/j.physd.2013.12.005>
23. A. R. Willms, P. M. Kitanov, W. F. Langford, Huygens' clocks revisited, *R. Soc. Open sci.* **4**, 170777 (2017). <https://doi.org/10.1098/rsos.170777>
24. F. Yen, C. dela Cruz, B. Lorenz, E. Galstyan, Y. Y. Sun, M. M. Gospodinov, C. W. Chu, Magnetic phase diagrams of multiferroic hexagonal  $\text{RMnO}_3$  (R = Er, Yb, Tm, and Ho), *J. Mater. Res.* **22**, 2163-2173 (2007).  
<https://doi.org/10.1557/jmr.2007.0271>
25. S. Kh. Estemirova, V. Ya. Mitrofanov, S. A. Uporov, G. A. Kozhina, Cationic nonstoichiometry, structural and magnetic properties of hexagonal  $\text{Tm}_{2-x}\text{Mn}_x\text{O}_3$  manganites, *J. Alloy. Comp.* **960**, 171084 (2023).  
<https://doi.org/10.1016/j.jallcom.2023.171084>
26. J. Schultheiß, L. Puntigam, M. Winkler, S. Krohns, D. Meier, H. Das, D. M. Evans, I. Kézsmárki, Magnetoelectric coupling at the domain level in polycrystalline hexagonal  $\text{ErMnO}_3$ , *Appl. Phys. Lett.* **124**, 252902 (2024).  
<https://doi.org/10.1063/5.0209216>
27. L. Meng, C. He, F. Yen, Magnetoelectric coupling based on protons in ammonium sulfate, *J. Phys. Chem. C* **124**, 17255-17261 (2020).  
<https://doi.org/10.1021/acs.jpcc.0c06048>
28. L. Meng, C. He, W. Ji, F. Yen, Magnetic properties of  $\text{NH}_4\text{H}_2\text{PO}_4$  and  $\text{KH}_2\text{PO}_4$ :

- Emergence of multiferroic salts, *J. Phys. Chem. Lett.* **11**, 8297-8301 (2020).  
<https://doi.org/10.1021/acs.jpcelett.0c02634>
29. C. W. Cheong, M. Mostovoy, Multiferroics: a magnetic twist for ferroelectricity, *Nat. Mat.* **6**, 13-20 (2007). <https://doi.org/10.1038/nmat1804>
30. Y. Y. Xu, L. Meng, M. M. Zhao, C. X. Peng, F. Yen, Electric polarization and magnetic properties of  $(\text{NH}_4)_{1-x}\text{K}_x\text{I}$  ( $x = 0.05\text{--}0.17$ ), *J. Alloy. Comp.* **960**, 170685 (2023). <https://doi.org/10.1016/j.jallcom.2023.170685>